Rare Metal Materials and Engineering
Volume 47, Suppl. 2, August 2018
Cite this article as: Rare Metal Materials and Engineering, 2018, 47(S2): 204-208.

Preparation of Porous Graphitic Carbon Nitride with Enhanced Visible-Light Photocatalytic Activities

You Zengyu[1], Su Yuxuan[1], Wang Hui[1], Yu Yang[1], Qin Tian[1], Shen Qianhong[1,2], Yang Hui[1,2]

[1] State Key Laboratory of Silicon Materials, Zhejiang University, Hangzhou 310027, China; [2] Zhejiang-California International NanoSystems Institute, Zhejiang University, Hangzhou 310058, China

Abstract: A simple and template-free synthesis method was developed to fabricate porous graphitic carbon nitride (g-C_3N_4) through a hydrothermal process in the presence of ammonium hydroxide. The effect of ammonium hydroxide on the structure of porous g-C_3N_4 was characterized by XRD, FT-IR, SEM and TEM. The photocatalytic activity of porous g-C_3N_4 was evaluated by the degradation of methylene blue (MB) under visible light irradiation. The results show that as-prepared porous g-C_3N_4 exhibits a porous nanostructure composed of 2D nanosheets and interconnected pores. The photocatalytic activity of porous g-C_3N_4 is enhanced, owing to the synergistic effect of more reaction sites and good separation efficiency of photo-generated carriers.

Key words: graphitic carbon nitride; porous structure; visible-light photocatalysis

As a promising way for environmental pollution purification, photocatalysis technology has been researched during the past decades. Although much progress have been made, low photocatalytic efficiency and poor utilization of sunlight still restrict further application of photocatalyst[1,2]. Since the year of 2009 when it has been proposed to be an visible-light driven photocatalyst, graphitic carbon nitride (g-C_3N_4) has drawn tremendous interest due to its metal-free composition, easy preparation and visible-light response (with a bandgap of 2.7 eV). Besides, 2D layer structure and tunable electronic structure make g-C_3N_4 a promising material for further research[3-7]. g-C_3N_4 can be simply prepared by the thermal condensation of several low-cost nitrogen-rich precursors such as cyanamide[7], dicyandiamide[8], melamine[9], urea[10] and mixtures thereof[11], which makes it a more accessible and promising photocatalyst. Nevertheless, g-C_3N_4 still suffered from some drawbacks such as small specific surface area, rapid recombination of photo-generated charge carriers and low transition efficiency[12]. Much work has been performed such as elements doping[13], constructing heterojunction between g-C_3N_4 and other semiconductors[14,15] to solve these problems. Besides, porous g-C_3N_4 with a large size is particularly attractive as an efficient photocatalyst recently, owing to its accessible porous framework, large specific surface area, and separability[16,17]. Moreover, because of rich surface functional groups and physicochemical properties, porous g-C_3N_4 can also act as an innovative catalyst support[18]. At present the template method was commonly used to form porous structure in g-C_3N_4, but it will make the preparation complicated as well as time-consuming.

Herein, we developed a simple and template-free synthesis method of porous g-C_3N_4 through a hydrothermal process in the presence of ammonium hydroxide. The effect of ammonium hydroxide on the structure of porous g-C_3N_4 was investigated. The photocatalytic activity of porous g-C_3N_4 under visible-light was evaluated by the degradation of methylene blue (MB). The relationships between the structural features, electronic properties, and photocatalytic activities of such structured g-C_3N_4 were also studied.

1 Experiment

All the chemicals including cyanamide, ammonium hydroxide and ethyl alcohol were used without any further purification. Firstly, a certain amount of cyanamide was placed in a semi-covered alumina crucible followed by being put into a tube furnace. Then the cyanamide was heated to 550 ^{o}C in air with a heating rate of 2.2 ^{o}C/min. After be-

Received date: August 25, 2017
Foundation item: National Key Research and Development Program of China (2016YFB0701100)
Corresponding author: Shen Qianhong, Ph. D., Associate Professor, School of Materials Science and Engineering, Zhejiang University, Hangzhou 310027, P. R. China, Tel: 0086-571-87951408, E-mail: s_qianhong@163.com

ing maintained at 550 °C for 4 h, the obtained g-C_3N_4 were cooled to room temperature naturally.

The as-prepared g-C_3N_4 (donated as CN) powder was put into a glass beaker with 50 mL deionized water. Then, a certain amount of $NH_3 \cdot H_2O$ was added to the system. After being stirred for 40 min, the mixture was transferred to a 100 mL teflon-lined steel autoclave. The autoclave was heated in an oven at 140 °C for 12 h. Subsequently, the precipitate was collected and washed by centrifugation with deionized water and ethyl alcohol two times and dried at 60 ℃ for 6 h. With the addition of $NH_3 \cdot H_2O$ during the hydrothermal process, the mixtures have different pH values (pH=8, 9, 10, 11, 12). Therefore, the corresponding products were donated as CN-8, CN-9, CN-10, CN-11 and CN-12, respectively.

X-ray power diffractometer (XRD, APEXII, Bruker, Germany) was used to identify the crystal structure of the samples. The 2θ ranged from 10 ° to 80 ° in step of 0.02 °. FT-IR spectra (Avatar 360, Nicolet, USA) were recorded in transmission mode from 4000 cm^{-1} to 400 cm^{-1} by the standard KBr disk method. Field emission scanning electron microscopy (SEM, SU-70, Hitachi, Japan) and field emission transmission electron microscopy (TEM, Tecnai G2 F20 S-TWIN, FEI, USA) were used to investigate the morphology of the samples. The photoluminescence spectra of samples were detected on a photoluminescence spectroscopy (PL, FLS920, Edinburgh, UK) with excitation wavelength of 325 nm. Electrochemical impedance spectroscopy was performed on an electrochemical station (EIS, CHI 660E, Chenhua, China). Photoelectric current (PC) response was obtained with the same electrochemical station (light on/off cycles: 40 s).

Photocatalytic activities of the as-prepared samples were evaluated by the degradation of methylene blue (MB) in aqueous solution under visible light irradiation. A 35 W metal-halide lamp (Philips) with a 420 nm UV-cutoff filter was used as light source and located 12 cm away from the surface of reaction solution (5 mW·cm^{-2}). In each experiment, 50 mg of a photocatalyst was dispersed in MB (100 mL, 10 mg·L^{-1}) aqueous solution. Prior to irradiation, the solution was continuously stirred in the dark for 2 h to achieve saturated absorption of MB onto the photocatalyst. During the photocatalytic reactions, the solution were kept magnetically stirring, and 5 mL of the mixture was collected at 30 min intervals followed by centrifugation (10000 r/min, 5 min) to remove the photocatalyst. The concentration of MB was determined by monitoring the change of optical density at 663 nm using a UV-Vis spectrophotometer (UV-3150, Shimadzu, Japan).

2 Results and Discussions

2.1 Structure and morphology

The crystal structures of as-prepared samples were characterized by X-ray diffraction patterns as shown in Fig.1a. Two pronounced diffraction peaks were observed at 13.2 ° and 27.4 ° corresponding to interlayer packing of tri-s-triazine units which is indexed as (110) and inter-planner stacking of conjugated aromatic systems which is indexed as (002), respectively[7]. The typical structure of g-C_3N_4 is not destroyed during the hydrothermal process as the main diffraction peaks of all products remain unchanged. However, the (002) peak of CN-12 exhibits an obvious shift to a higher angle, which suggests that it has a more-condensed layer structure[17]. Furthermore, the (002) peak intensity of CN-12 decreases significantly, confirming the formation of porous nanostructure composed of nanosheets and interconnected pores[19]. The structures of as-prepared samples are also characterized by FT-IR spectra as shown in Fig.1b. The peak at 800 cm^{-1} is attributed to triazine units while the set of peaks between 1200 to 1600 cm^{-1} correspond to the typical stretching vibration modes of C—N and C≡N heterocycles[15]. The results further confirm that the typical structure of g-C_3N_4 is unchanged after the hydrothermal process.

The morphology and structure were directly observed by SEM images. As shown in Fig.2a and Fig.2b, the morphologies of CN-8 and CN-9 are mainly to be bulk like with few fragments on the surface. With the addition of ammonium hydroxide increasing, g-C_3N_4 nanosheets and pore structure can be observed in CN-10 and CN-11 (Fig.2c and Fig.2d), while CN-12 exhibits a porous nanostructure that is composed of 2D nanosheets and interconnected pores. As shown in Fig.2f, interconnected pores structure of CN-12 can be observed obviously. The nanosheets of g-C_3N_4 have a thickness of about 20 nm which is corresponding to SEM images. This unique structure may offer more sites that are beneficial for transfer efficiency of photo-generated electro-hole pairs. The formation of this porous structure may be due to the assistance of ammonium hydroxide during hydrothermal process. Firstly, the bubble of NH_3 offered by ammonium hydroxide can act as a template facilitating the formation pore structure[20]. Secondly, bulk-like g-C_3N_4 can be exfoliated into nanosheets by hydrothermal treatment with the aid of ammonium hydroxide[21]. Consequently, CN-12 with porous nanostructure composed of 2D nanosheets and interconnected pores are obtained.

2.2 Optical property

The intensity of PL emission spectra indicates the recombination speed of photo-generated electron-hole pairs. As shown in Fig.3, CN has a strong emission peak at around 460 nm. Obviously, the emission peak of CN-12 has a little higher intensity and a blue shift caused by its unique structure. 2D g-C_3N_4 nanosheets in CN-12 have a larger bandgap than bulk g-C_3N_4, which is attributed to the quantum confinement effect. The conduction and valence band edge are shifted in opposite directions, leading to the blue shift and higher intensity[12].

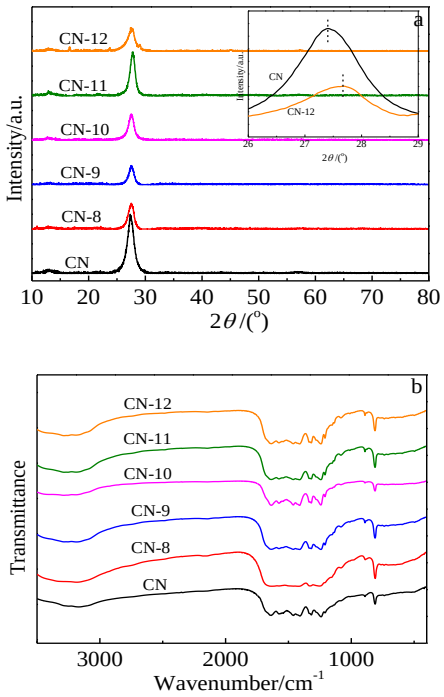

Fig.1 XRD patterns (a) and FT-IR spectra (b) of as-prepared samples

2.3 Photoelectrochemical properties

Electrochemical experiments have been performed to further investigate the photo-generated charge transfer and separation behaviors. Fig.4a exhibits transient photocurrent responses via repeated on/off visible light irradiation cycles of CN and CN-12 electrodes in a 0.5 mol/L Na_2SO_4 aqueous solution, which can demonstrate the separation and migration efficiency of photo-generated carriers[22]. Both CN and CN-12 exhibit reversible photocurrent responses on each illumination. The transient photocurrent of CN-12 is higher than that of CN, clearly confirming that the well-constructed porous structure of CN-12 has a significant improvement in suppressing charge recombination and transferring the photo-generated electrons.

Electrochemical impendence spectroscopy (EIS) was conducted to further investigate the charge transport behavior of CN-12. EIS Nyquist plots of CN and CN-12 electrodes in a 0.5 mol/L Na_2SO_4 aqueous solutions before and after visible-light irradiation are shown in Fig.4b. In the Nyquist diagram, a smaller arc radius suggests an effective separation of photo-generated electron-hole pairs and fast interfacial charge transfer[23]. Both CN and CN-12 show a smaller arc radius after light irradiation than that before light irradiation illustrating a better charge transfer efficiency in light. However, CN-12 exhibits smaller charge transfer resistance than CN both before and after light irradiation, which suggests a predictable higher photocatalytic activity.

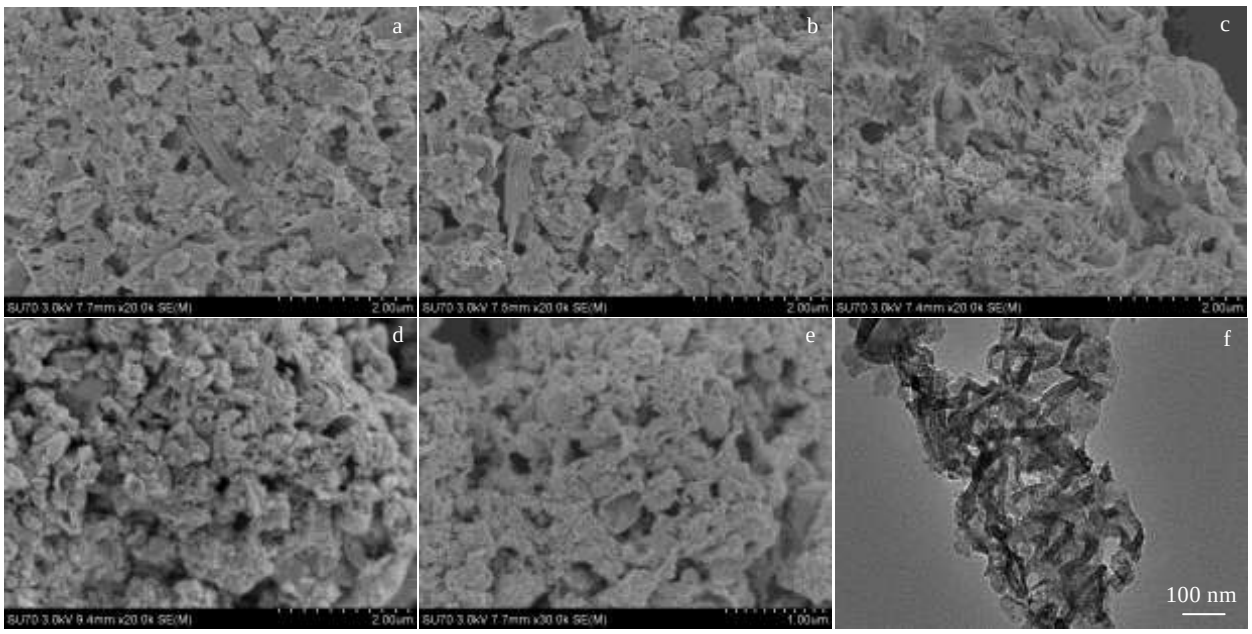

Fig.2 SEM images of CN-8 (a), CN-9 (b), CN-10 (c), CN-11 (d) and CN-12 (e); (f) TEM image of CN-12

2.4 Photocatalytic activities

The photocatalytic activities of the as-obtained samples were evaluated through the photocatalytic degradation of methylene blue (MB) under visible light irradiation (λ>420 nm). As shown in Fig.5a, the blank test illustrates that MB is stable under visible light irradiation if there is no photocatalyst. As the addition of ammonium hydroxide increases during hydrothermal process, CN-8, CN-9 and CN-10 show higher photocatalytic activities than CN, owing to the partly formed porous structure. When further increasing the addition of ammonium hydroxide, CN-11 exhibits a further enhancement. As suggested in the degradation dia-

g r a m , that depend on the separation efficiency and migration ability

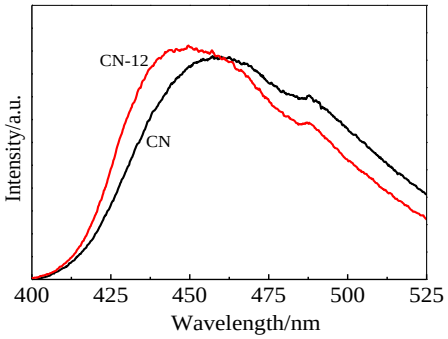

Fig.3 PL spectra of CN and CN-12

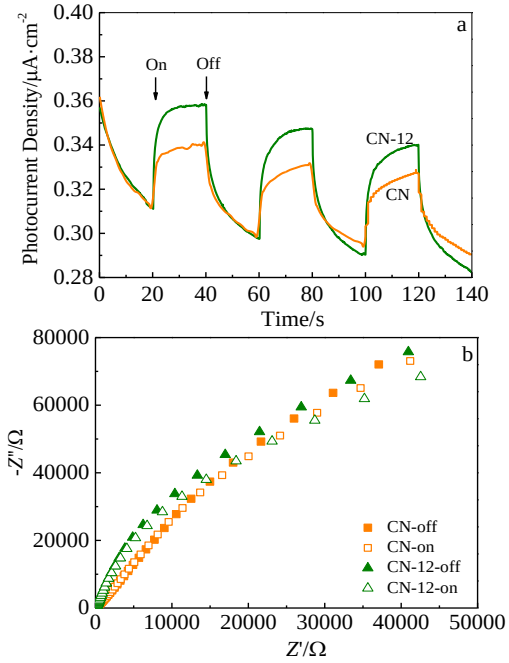

Fig.4 Photoelectrochemical properties of CN and CN-12: (a) periodic ON/OFF photocurrent and (b) electrochemical impedance spectroscopy Nyquist plots

CN-12 exhibits the highest photocatalytic activities of all the as-prepared samples owing to the well formation of porous structure. The photocatalytic decomposition kinetics of as-prepared samples is fitted by a pseudo-first-order model. As demonstrated in Fig.5b, CN-12 exhibits the highest photocatalytic decomposition rate of 0.078 h^{-1}, much higher than CN (0.011 h^{-1}). This result can be attributed to the well-architected structure of CN-12 and explained as follows: Firstly, porous structure of CN-12 which is constructed by g-C_3N_4 nanosheets and interconnected pores suggests more active sites to accelerate the photocatalytic degradation. Secondly, photocatalytic reaction is determined by radicals

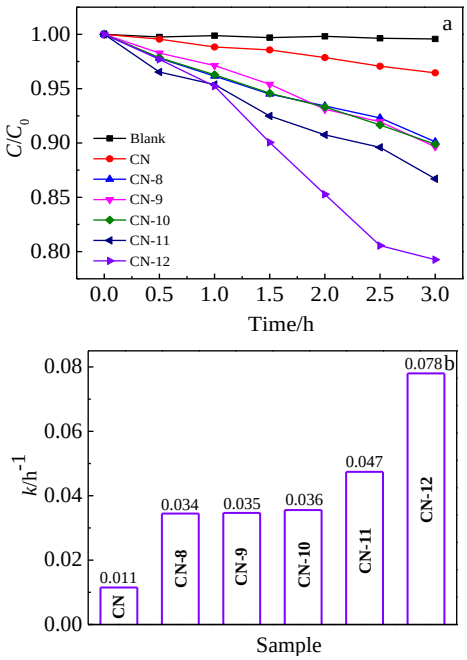

Fig.5 Photocatalysis analysis of the as-prepared samples: (a) photocatalytic degradation of MB and (b) the corresponding kinetics (photocatalytic decomposition rate, *k*)

of photo-generated electrons. As above evidence indicating, CN-12 exhibits significant enhancement in suppressing charge recombination and transferring the photo-induced electrons.

3 Conclusions

1) Porous g-C_3N_4 has been synthesized via a hydrothermal process in the presence of ammonium hydroxide. The released NH_3 can act as a template during the formation process.

2) The exfoliation effect of ammonium hydroxide towards bulk g-C_3N_4 facilitates the formation of g-C_3N_4 nanosheets which constitute CN-12 together with interconnected pores.

3) The CN-12 exhibits an obviously enhanced visible-light photocatalytic activity compared with bulk g-C_3N_4, owing to more reaction sites and high separation efficiency of carriers.

References

1 Forgacs E, Cserhati T, Oros G. *Environment International*[J], 2004, 30(7): 953
2 Liang Q H, Li Z, Yu X L *et al. Advanced Materials*[J], 2015, 27(31): 4634
3 Liu J, Liu Y, Liu N Y *et al. Science*[J], 2015, 347(6225): 970
4 Zheng Y, Liu J, Liang J *et al. Energy & Environmental Sci-*

ence[J], 2012, 5(5): 6717
5 Wang Y, Wang X C, Antonietti M. *Angewandte Chemie International Edition*[J], 2012, 51(1): 68
6 Cao S W, Low J X, Yu J G *et al. Advanced Materials*[J], 2015, 27(13): 2150
7 Wang X C, Maeda K, Thomas A *et al. Nature Materials*[J], 2009, 8(1): 76
8 Zhang G G, Zhang M W, Ye X X *et al. Advanced Materials*[J], 2014, 26(5): 805
9 Guo Y, Li J H, Gao Z Q *et al. Applied Catalysis B: Environmental*[J], 2016, 192: 57
10 Dong F, Wang Z Y, Sun Y J *et al. Journal of Colloid and Interface Science*[J], 2013, 401: 70
11 Jorge A B, Martin D J, Dhanoa M T S *et al. The Journal of Physical Chemistry C*[J], 2013, 117(14): 7178
12 Niu P, Zhang L L, Liu G *et al. Advanced Functional Materials*[J], 2012, 22: 4763
13 Zhang Y J, Mori T, Ye J H *et al. Journal of the American Chemical Society*[J], 2010, 132(18): 6294
14 Shen J C, Yang H, Shen Q H *et al. CrystEngComm*[J], 2014, 16(10): 1868
15 Feng Y, Shen J C, Cai Q F *et al. New Journal of Chemistry*[J], 2015, 39(2): 1132
16 Zhang Y, Zhu P Q, Chen L *et al. Journal of Materials Chemistry A*[J] 2014, 2(30): 11 966
17 Shen J C, Yang H, Shen Q H *et al. European Journal of Inorganic Chemistry*[J], 2015, 15: 2611
18 Li X H, Wang X C, Antonietti M. *Chemical Science*[J], 2012, 3(6): 2170
19 Yang S B, Gong Y J, Zhang J S *et al. Advanced Materials*[J], 2013, 25(17): 2452
20 Wang S P, Li C J, Wang T *et al. Journal of Materials Chemistry A*[J], 2014, 2(9): 2885
21 Zhang X D, Wang H X, Wang H *et al. Advanced Materials*[J], 2014, 26(26): 4438
22 Li Y L, Wang J S, Yang Y L *et al. Journal of Hazardous Materials*[J], 2015, 292: 79
23 Bai X J, Wang L, Wang Y J *et al. Applied Catalysis B: Environmental*[J], 2014, 152-153: 262

多孔类石墨相氮化碳的制备及光催化性能研究

尤增宇[1]，苏钰璇[1]，王　辉[1]，于　洋[1]，秦　天[1]，申乾宏[1,2]，杨　辉[1,2]
(1. 浙江大学 硅材料国家重点实验室，浙江 杭州 310027)
(2. 浙江大学 浙江加州国际纳米技术研究院，浙江 杭州 310058)

摘　要：通过简单的氨水水热法制备得到了多孔 g-C_3N_4 光催化材料。利用 X 射线衍射（XRD）、红外光谱（FT-IR）、扫描电子显微镜（SEM）、透射电子显微镜（TEM）研究了氨水对多孔 g-C_3N_4 结构的影响。并以亚甲基蓝为目标分解物考察了样品的可见光催化活性。结果表明：制备得到多孔 g-C_3N_4 具有由 2D 纳米片和相互连通的孔道组成的多孔纳米结构。多孔 g-C_3N_4 的可见光催化活性得到了提升，原因在于相较于普通 g-C_3N_4，多孔 g-C_3N_4 能够提供更多的光催化反应活性位点，并且具有更高的光生载流子分离及迁移效率。

关键词：g-C_3N_4；多孔结构；可见光催化

作者简介：尤增宇，男，1989 年生，博士生，浙江大学材料科学与工程学院，浙江 杭州 310027，电话：0571-87953313，E-mail: youzengyu@zju.edu.cn